

Hybrid Digital-Analog Beamforming and MIMO Radar with OTFS Modulation

Lorenzo Gaudio¹, Mari Kobayashi², Giuseppe Caire³, Giulio Colavolpe¹

¹University of Parma, Italy

²Technical University of Munich, Munich, Germany

³Technical University of Berlin, Germany

Emails: lorenzo.gaudio@studenti.unipr.it, mari.kobayashi@tum.de, giulio.colavolpe@unipr.it, caire@tu-berlin.de

Abstract—Motivated by future automotive applications, we study some joint radar target detection and parameter estimation problems where the transmitter, equipped with a mono-static MIMO radar, wishes to detect multiple targets and then estimate their respective parameters, while simultaneously communicating information data using orthogonal time frequency space (OTFS) modulation. Assuming that the number of radio frequency chains is smaller than the number of antennas over the mmWave frequency band, we design hybrid digital-analog beamforming at the radar transmitter adapted to different operating phases. The first scenario considers a wide angular beam in order to perform the target detection and parameter estimation, while multicasting a common message to all possible active users. The second scenario considers narrow angular beams to send information streams individually to the already detected users and simultaneously keep tracking of their respective parameters. Under this setup, we propose an efficient maximum likelihood scheme combined with hybrid beamforming to jointly perform target detection and parameter estimation. Our numerical results demonstrate that the proposed algorithm is able to reliably detect multiple targets with a sufficient number of antennas and achieves the Cramér-Rao lower bound for radar parameter estimation such as delay, Doppler and angle-of-arrival (AoA).

Index Terms—OTFS, MIMO radar, joint radar parameter estimation and communication, maximum likelihood detection.

I. INTRODUCTION

Multiple-input multiple-output (MIMO) radar has been extensively studied and was shown to improve the resolution, i.e., the ability to distinguish multiple targets, thanks to the additional spatial dimension (see, e.g., [1]). A careful design of beamforming (BF), or power allocation along angular directions, is crucial to achieve accurate radar detection and parameter estimation performance. This is particularly relevant to automotive radar [2] operating over millimeter wave (mmWave) frequency bands, as the high propagation loss must be compensated by proper BF, or more generally beam alignment both at transmitter (Tx) and receiver (Rx) sides (see e.g. [3] and references therein). Note that, in a mono-static radar system with co-located Tx and Rx, transmit and receive antennas are calibrated such that their beam patterns “look in the same direction”. Moreover, BF at the radar Tx might be adaptive, depending on different operating phases (see e.g., [4], [5] and references therein). Namely, the transmitted power shall be allocated to wider angular sectors during a target detection/search phase, while narrow and distinct

beams, each focused on the detected target, shall be used to minimize “multi-target” interference in a tracking phase [1], [6], [7]. During the target detection phase, a non-trivial tradeoff appears. On one hand, a wider angular sector coverage enables to detect potentially more targets if the received backscattered power is high enough. On the other hand, a directional BF grants higher received signal-to-noise ratio (SNR), at the cost of a time-consuming search over narrower angular sectors (as classical radar successively swapping adjacent regions, see, e.g., [6]). Different solutions to the aforementioned problem can be found in the literature (see, e.g., [5], [8], [9], [10]).

As an extension of our previous works [11], [12], this paper studies the joint target detection and parameter estimation problem with a mono-static MIMO radar adopting orthogonal time frequency space (OTFS), i.e., a multi-carrier modulation proposed in [13] and already studied in different MIMO configurations (see, e.g., [14], [15]). The use of communication waveforms for radar has been motivated by the joint radar and communication paradigm, where two functions are implemented by sharing the same resources and the same waveform (see e.g. [16], [17], [18] and references therein). Contrary to the existing works on radar sensing using OTFS [11], [12], [19], this paper considers MIMO radar under a practical mmWave system architecture such that the number of radio frequency (RF) chains (N_{rf}) is much smaller than the number of antennas (N_a). In fact, it is difficult to implement a fully digital BF, or, equivalently, associate one RF chain per antenna (including A/D conversion, modulation, and amplification) in a small form factor and highly integrated technology over a large signal bandwidth. Therefore, focusing on mmWave automotive applications, we consider hybrid digital-analog (HDA) BF schemes as typically considered in the literature (see, e.g., [20], [21] and references therein). We will study two different scenarios, exploring the aforementioned BF tradeoff. The first scenario considers a Tx BF design such that the beam covers a wide angular sector, to perform target detection and parameter estimation, while multicasting a common message to all possible active users (see Fig. 1a). The common message corresponds, for instance, to real-time traffic information that can be sent by a base station nearby or a car itself. Assuming that this initial communication phase is established, the second scenario considers a Tx BF with directed narrow beams, such that individual information streams are sent to the detected users (see Fig. 1b). Note that the Radar Rx uses a wide beam

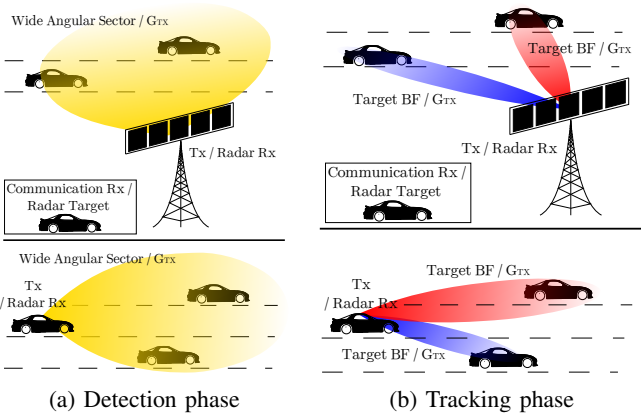


Fig. 1: Two scenarios with two different Tx beam patterns. In (a), a Tx (a base station or a car) broadcasts a common message exploring a wide angular sector. In (b), we consider directional BF towards the detected targets. The Rx always makes use of a wide beam within the angular sector of interest.

pattern consisting of N_{rf} beams as illustrated in Fig. 2 to obtain a meaningful vector observation, necessary for angle of arrival (AoA) estimation, regardless of the operating phase. This is in a sharp contrast to the hybrid beam alignment considered in the communication system where the receiver also applies BF and obtains a scalar observation precluding the estimation of the AoA (see, e.g., [20], [3] and references therein).

Under this setup, we propose an efficient maximum likelihood (ML)-based scheme combined with HDA BF to jointly perform target detection and parameter estimation. More precisely, our scheme first performs target detection and super-resolution estimation of delay, Doppler shift, and AoA using a wide angular beam along which a single data stream is sent. Then, once the targets are detected, the subsequent tracking phase performs the parameter estimation using multiple narrow beams along which multiple data streams can be sent. Our numerical results demonstrate that the proposed scheme is able to reliably detect multiple targets while essentially achieving the Cramér-Rao Lower Bound (CRLB) for radar parameter estimation. Furthermore we investigate various scenarios of near-far effects of targets, showing that a successive interference cancellation (SIC) mechanism is able to efficiently remove the masking effect between targets located at different ranges from the radar, and we provide an in-deep analysis of the two scenarios of interest, showing their limits and advantages.

The paper is organized as follows. In Section II we introduce the physical model and OTFS modulation basics. Section III exploits the joint detection and parameter estimation algorithm. Numerical results are analyzed in Section IV, and Section V concludes the paper.

We adapt the following notations. $(\cdot)^{\text{T}}$ denotes the transpose operation. $(\cdot)^{\text{H}}$ denotes the Hermitian (conjugate and transpose) operation. Operator $|\cdot|$ denotes the absolute value $|x|$ if $x \in \mathbb{R}$, or the cardinality (number of elements) of a discrete set, i.e., $|\mathcal{F}|$, if \mathcal{F} is a discrete set.

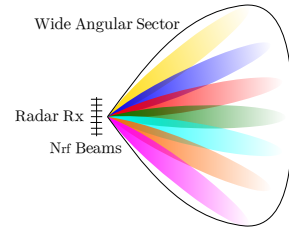


Fig. 2: Beam configuration at the radar Rx for the two scenarios depicted in Fig. 1. N_{rf} beams cover a wide angular sector.

II. PHYSICAL MODEL

We consider joint radar detection and parameter estimation in a system operating over a channel bandwidth B at the carrier frequency f_c . We assume a Tx equipped with a mono-static MIMO radar with N_a antennas and N_{rf} RF chains, operating in full-duplex mode.¹ The radar Rx (which is colocated with the Tx) processes the backscattered signal to identify the presence of targets within the beam, while estimating parameters of interest such as range, velocity, and AoA. A point target model is taken into account, such that each target can be represented through its line-of-sight (LoS) path only [25], [26], [9]. By letting $\phi \in [-\frac{\pi}{2}, \frac{\pi}{2}]$ be the steering angle, by considering an antenna array with $\lambda/2$ spacing (λ is the wavelength), the Tx and Rx arrays are given by $\mathbf{a}(\phi)$ and $\mathbf{b}(\phi)$ respectively, where $\mathbf{a}(\phi) = (a_1(\phi), \dots, a_{N_a}(\phi))^{\text{T}} \in \mathbb{C}^{N_a}$, denotes the uniform linear array response vector of the radar Rx with

$$a_n(\phi) = e^{j(n-1)\pi \sin(\phi)}, \quad n = 1, \dots, N_a, \quad (1)$$

and $b_n(\phi) = a_n(\phi)$. Under the mono-static radar assumption, i.e., same angle ϕ at radar Tx and Rx, vectors \mathbf{a} and \mathbf{b} result to be equal. The channel is modeled as a P -tap time-frequency selective channel of dimension $N_a \times N_a$ given by [27]

$$\mathbf{H}(t, \tau) = \sum_{p=0}^{P-1} h_p \mathbf{b}(\phi_p) \mathbf{a}^{\text{H}}(\phi_p) \delta(\tau - \tau_p) e^{j2\pi \nu_p t}, \quad (2)$$

where P is the number of targets, h_p is a complex channel gain including the pathloss, $\nu_p = \frac{2v_p f_c}{c}$ is the round-trip Doppler shift, $\tau_p = \frac{2r_p}{c}$ is the round-trip delay, and ϕ_p denotes the AoA, each corresponding to the p -th target, respectively.

A. OTFS Input Output Relation

We consider OTFS with M subcarriers of bandwidth Δf each, such that the total bandwidth is given by $B = M\Delta f$. We let T denote the symbol time, yielding the OTFS frame duration of NT , with N number of symbols in time. We let $T\Delta f = 1$, as typically considered in the OTFS literature [11], [13], [28]. In order to consider the aforementioned different operational modes, we let N_s denote the number of data streams to be sent per time-frequency domain such that $N_s = 1$ corresponds to the multicasting of a single data stream and $N_s \leq N_{\text{rf}}$ corresponds to the broadcasting of individual data

¹Full-duplex operations can be achieved with sufficient isolation between the transmitter and the (radar) detector and possibly interference analog pre-cancellation in order to prevent the (radar) detector saturation [22], [23], [24].

streams. Following the standard derivation of the input-output relation of OTFS (see, e.g., [13], [11]), N_s -dimensional data symbols $\{\mathbf{x}_{k,l}\}$, for $k = 0, \dots, N-1$, $l = 0, \dots, M-1$, belonging to any constellation, are arranged in an $N \times M$ two-dimensional grid referred to as the Doppler-delay domain, i.e., $\Gamma = \{(k/NT, l/M\Delta f)\}$. The Tx first applies the inverse symplectic finite Fourier transform (ISFFT) to convert data symbols $\{\mathbf{x}_{k,l}\}$ into a $N_s \times 1$ block $\{\mathbf{X}[n, m]\}$ in the time-frequency domain

$$\mathbf{X}[n, m] = \sum_{k=0}^{N-1} \sum_{l=0}^{M-1} \mathbf{x}_{k,l} e^{j2\pi(\frac{nk}{N} - \frac{ml}{M})}, \quad (3)$$

for $n = 0, \dots, N-1$, $m = 0, \dots, M-1$, satisfying the average power constraint $\mathbb{E}[\mathbf{X}[n, m]\mathbf{X}[n, m]^H] = P_{\text{avg}}/(NMN_a)\mathbf{I}_{N_s}$, where \mathbf{I}_{N_s} denotes an identity matrix of dimension N_s . After assigning N_s streams to N_{rf} RF chains through a mapping matrix $\mathbf{V} \in \mathbb{C}^{N_{\text{rf}} \times N_s}$, the Tx generates the N_{rf} -dimensional continuous-time signal

$$\mathbf{s}(t) = \mathbf{V} \sum_{n=0}^{N-1} \sum_{m=0}^{M-1} \mathbf{X}[n, m] g_{\text{tx}}(t - nT) e^{j2\pi m \Delta f (t - nT)}. \quad (4)$$

Since the number of RF chains is typically much smaller than the number of antennas, different types of HDA architectures between RF chains and antennas have been considered in the literature (see e.g. [20]). In this paper, we focus on the fully-connected HDA scheme of [20]. For any HDA architecture, the transmitter applies the hybrid BF matrix denoted by $\mathbf{F} \in \mathbb{C}^{N_a \times N_{\text{rf}}}$ that captures both baseband and RF analog BF (see [4], [10]), while the receiver sees the received signal of a reduced dimension through a projection matrix denoted by $\mathbf{U} \in \mathbb{C}^{N_{\text{rf}} \times N_a}$. By imposing $\text{tr}(\mathbf{F}\mathbf{V}\mathbf{V}^H\mathbf{F}^H) = N_a$, the total power constraint P_{avg} is satisfied.

By transmitting the signal (4) over the channel (2), the N_{rf} -dimensional continuous-time received signal is given by

$$\mathbf{r}(t) = \sum_{p=0}^{P-1} h_p \mathbf{U} \mathbf{b}(\phi_p) \mathbf{a}^H(\phi_p) \mathbf{F} \mathbf{s}(t - \tau_p) e^{j2\pi \nu_p t}. \quad (5)$$

The output of the Rx filter-bank adopting a generic receive shaping pulse $g_{\text{rx}}(t)$ is given in (6), shown at the top of next page. By sampling at $t = nT$ and $f = m\Delta f$, we obtain

$$\mathbf{y}[n, m] = \mathbf{y}(t, f)|_{t=nT}^{f=m\Delta f} = \sum_{n'=0}^{N-1} \sum_{m'=0}^{M-1} \mathbf{h}_{n,m}[n', m'], \quad (7)$$

where the time-frequency domain input-output relation $\mathbf{h}_{n,m}[n', m']$ is given in (8), shown at the top of next page. Notice that we defined the cross ambiguity function $C_{u,v}(\tau, \nu) \triangleq \int_{-\infty}^{\infty} u(s)v^*(s-\tau)e^{-j2\pi\nu s} ds$ as in [30], let $h'_p = h_p e^{j2\pi\nu_p \tau_p}$, and imposed the term $e^{-j2\pi m m' \Delta f T} = 1$, $\forall n', m$, under the hypothesis $T\Delta f = 1$. Since each $X_i[n, m]$ is generated via ISFFT, the received signal in the delay-Doppler domain is obtained by the application of the symplectic finite Fourier transform (SFFT)

$$\mathbf{y}[k, l] = \sum_{n,m} \frac{\mathbf{y}[n, m]}{NM} e^{j2\pi(\frac{ml}{M} - \frac{nk}{N})} = \sum_{k', l'} \mathbf{g}_{k,k'}[l, l'], \quad (9)$$

where the inter-symbol interference (ISI) coefficient of the Doppler-delay pair $[k', l']$ seen by sample $[k, l]$ is given by

$$\mathbf{g}_{k,k'}[l, l'] = \sum_p h'_p \mathbf{U} \mathbf{b}(\phi_p) \mathbf{a}^H(\phi_p) \mathbf{F} \mathbf{V} \mathbf{x}_{k', l'} \Psi_{k,k'}^p[l, l'], \quad (10)$$

with $\Psi_{k,k'}^p[l, l']$ defined in (11), shown at the top of next page. A simplified version of $\Psi_{k,k'}^p[l, l']$ obtained by approximating the cross ambiguity function can be found in [11].

B. Beamforming matrices

The design of BF matrix \mathbf{F} at the radar Tx depends on the operating phase. During the detection phase depicted in Fig. 1a, we choose \mathbf{F} for a given angular sector such that both Tx and Rx are aligned towards the same wide angular sector. Following [4, Section III.C], we construct $\mathbf{F} \in \mathbb{C}^{N_a \times N_{\text{rf}}}$ to cover a wide angular sector $[-\theta, \theta]$ as follows. By representing this angular sector by a discrete set of N_{rf} angles, denoted by $\Theta = \{\pm(\theta/(2N_{\text{rf}}) + k\theta/N_{\text{rf}})\}$, for $k = 0, \dots, N_{\text{rf}}/2 - 1$, we construct each column of $\mathbf{F} = [\mathbf{f}_1, \dots, \mathbf{f}_{N_{\text{rf}}}]$ as

$$\mathbf{f}_i = \frac{\mathbf{a}(\theta_i)}{|\mathbf{a}(\theta_i)|}, \quad i = 1, \dots, N_{\text{rf}}, \quad (12)$$

with a suitable normalization, where $\mathbf{a}(\theta_i)$ is defined in (1).

During the target tracking phase, we form multiple narrow beams corresponding to the estimated AoA of the detected targets. This is illustrated with red and blue beams, corresponding to two different AoA, in Fig. 1b. Assuming that P targets are detected and their respective AoA are estimated, we construct \mathbf{F} by replacing θ_i by $\hat{\phi}_p$ for the first P columns in (12) [4, Section III.B].

Contrary to the transmit beamforming matrix, the reduction matrix \mathbf{U} at the radar Rx remains the same for both detection and tracking phases. Namely, we set $\mathbf{U} = \mathbf{F}^H$, where each column is given in (12). This is illustrated in Fig. 2. This choice of an isotropic receive beam enables to obtain a multi-dimensional signal for AoA estimation in both detection and tracking phases.

III. JOINT DETECTION AND PARAMETERS ESTIMATION

We wish to estimate the set of four parameters $\boldsymbol{\theta} = \{h'_p, \phi_p, \tau_p, \nu_p\} \in \mathcal{T}^P$, with $\mathcal{T} = \mathbb{C} \times \mathbb{R} \times \mathbb{R} \times \mathbb{R}$. By defining

$$\mathbf{G}_p(\tau_p, \nu_p, \phi_p) \triangleq (\mathbf{U} \mathbf{b}(\phi_p) \mathbf{a}^H(\phi_p) \mathbf{F} \mathbf{V}) \otimes \Psi^p, \quad (13)$$

where \otimes is the Kronecker product,² as the $N_{\text{rf}}NM \times N_sNM$ matrix obtained by multiplying Ψ^p by a different coefficient of $(\mathbf{U} \mathbf{b}(\phi_p) \mathbf{a}^H(\phi_p) \mathbf{F} \mathbf{V})$. Thus, by stacking \mathbf{X} into a N_sNM -dimensional vector \mathbf{x} and defining an output vector \mathbf{y} of dimension $NMN_{\text{rf}} \times 1$, the received signal in the presence of noise is given by

$$\mathbf{y} = \sum_{p=0}^{P-1} [h'_p \mathbf{G}_p(\tau_p, \nu_p, \phi_p)] \mathbf{x} + \mathbf{w}, \quad (14)$$

where \mathbf{w} denotes the additive white Gaussian noise (AWGN) vector with independent and identically distributed entries

²Note that $\mathbf{A}^{X \times Y} \otimes \mathbf{B}^{Z \times K} = \mathbf{C}^{XZ \times YK}$.

$$\begin{aligned} \mathbf{y}(t, f) &= \int \mathbf{r}(t') g_{\text{rx}}^*(t' - t) e^{-j2\pi f t'} dt' = \int_{t'} g_{\text{rx}}^*(t' - t) \sum_{p=0}^{P-1} h_p \mathbf{U}\mathbf{b}(\phi_p) \mathbf{a}^{\text{H}}(\phi_p) \mathbf{F}\mathbf{s}(t' - \tau_p) e^{j2\pi\nu_p t'} e^{-j2\pi f t'} dt' \\ &= \sum_{p, n', m'} h_p \mathbf{U}\mathbf{b}(\phi_p) \mathbf{a}^{\text{H}}(\phi_p) \mathbf{F}\mathbf{V}\mathbf{X}[n', m'] \int_{t'} g_{\text{rx}}^*(t' - t) g_{\text{tx}}(t' - \tau_p - n'T) e^{j2\pi m' \Delta f (t' - \tau_p - n'T)} e^{j2\pi(\nu_p - f)t'} dt' \end{aligned} \quad (6)$$

$$\mathbf{h}_{n, m}[n', m'] = \sum_{p=0}^{P-1} h'_p \mathbf{U}\mathbf{b}(\phi_p) \mathbf{a}^{\text{H}}(\phi_p) \mathbf{F}\mathbf{V}\mathbf{X}[n', m'] C_{g_{\text{tx}}, g_{\text{rx}}}((n - n')T - \tau_p, (m - m')\Delta f - \nu_p) e^{j2\pi n' T \nu_p} e^{-j2\pi m \Delta f \tau_p} \quad (8)$$

$$\Psi_{k, k'}^p[l, l'] = \sum_{n, n', m, m'} \frac{C_{g_{\text{tx}}, g_{\text{tx}}}((n - n')T - \tau_p, (m - m')\Delta f - \nu_p)}{NM} e^{j2\pi n' T \nu_p} e^{-j2\pi m \Delta f \tau_p} e^{j2\pi \left(\frac{n'k'}{N} - \frac{m'l'}{M}\right)} e^{-j2\pi \left(\frac{nk}{N} - \frac{ml}{M}\right)} \quad (11)$$

of zero mean and variance σ_w^2 . The problem reduces to detect P targets and estimate the $4P$ associated parameters (complex channel coefficient, Doppler, delay, and angle) from the $N_{\text{rf}}MN$ -dimensional received signal. To this end, we define the ML function as

$$l(\mathbf{y}|\boldsymbol{\theta}, \mathbf{x}) = \left| \mathbf{y} - \sum_p h'_p \mathbf{G}_p \mathbf{x} \right|^2, \quad (15)$$

where we use the short hand notation $\mathbf{G}_p \triangleq \mathbf{G}(\tau_p, \nu_p, \phi_p)$. The ML solution is given by

$$\hat{\boldsymbol{\theta}} = \arg \min_{\boldsymbol{\theta} \in \mathcal{T}^P} l(\mathbf{y}|\boldsymbol{\theta}, \mathbf{x}). \quad (16)$$

For a fixed set of $\{\phi_p, \tau_p, \nu_p\}$, the ML estimator of $\{h'_p\}$ is given by solving the following set of equations

$$\mathbf{x}^{\text{H}} \mathbf{G}_p^{\text{H}} \left(\sum_{q=0}^{P-1} h'_q \mathbf{G}_q \right) \mathbf{x} = \mathbf{x}^{\text{H}} \mathbf{G}_p^{\text{H}} \mathbf{y}, \quad p = 0, \dots, P-1. \quad (17)$$

By plugging (17) into (15), it readily follows that minimizing $l(\mathbf{y}|\boldsymbol{\theta}, \mathbf{x})$ reduces to maximize the following function

$$\begin{aligned} l_2(\mathbf{y}|\boldsymbol{\theta}, \mathbf{x}) &= \sum_p h'_p \mathbf{y}^{\text{H}} \mathbf{G}_p \mathbf{x} \\ &= \sum_p S_p(\tau_p, \nu_p, \phi_p) - I_p(\{h'_q\}_{q \neq p}, \boldsymbol{\theta}), \end{aligned} \quad (18)$$

where $S_p(\tau_p, \nu_p, \phi_p)$ and $I_p(\{h'_q\}_{q \neq p}, \boldsymbol{\theta})$ (S_p and I_p in short hand notation) denote the useful signal and the interference term for target p , given respectively by

$$S_p = \frac{|\mathbf{y}^{\text{H}} \mathbf{G}_p \mathbf{x}|^2}{|\mathbf{G}_p \mathbf{x}|^2}, \quad (19)$$

$$I_p = \frac{(\mathbf{y}^{\text{H}} \mathbf{G}_p \mathbf{x}) \mathbf{x}^{\text{H}} \left(\mathbf{G}_p^{\text{H}} \sum_{q \neq p} h'_q \mathbf{G}_q \right) \mathbf{x}}{|\mathbf{G}_p \mathbf{x}|^2}. \quad (20)$$

Notice that we have $I_p = 0$ if there is only one target.

A. Successive Interference Cancellation (SIC) and Joint Target Detection and Parameters Estimation Algorithm

The use of OTFS for radar tasks introduces some limitations. In particular, OTFS with $T\Delta f = 1$ yields a cross ambiguity function $C_{g_{\text{tx}}, g_{\text{rx}}}(\tau, \nu)$ that incurs significant side-lobes in the Doppler-delay domain. As a result, our simulations show that the magnitude of the useful signal, i.e., $\max_{(\tau, \nu)} S_p(\tau, \nu, \phi)$, has a main lobe around the angle ϕ_p of target p and non-negligible side-lobes in the angular domain. Since the signal magnitude strictly depends on the received backscattered power, the sidelobes of a strong target, closer to the radar, may completely mask the main lobe of weaker targets, far from the radar. Therefore, situations of near-far effect among the targets, causing large power imbalance in the backscatter waves, must be handled explicitly by some additional signal processing. This motivates us to incorporate SIC in our ML-based target detection. Given the received signal in (14), once a strong target is detected and its radar parameters are estimated, its contribution, and thus the masking effect, can be removed from the received signal (see (24) in Algorithm 1). This process can be run iteratively to cancel the contributions of new detected targets, until a given condition or stopping criteria is satisfied (e.g., a target is found in an angular sector already explored, or the magnitude of the useful signal goes below a certain value). Algorithm 1 describes the steps to perform joint detection and radar parameters estimation. Some remarks on Algorithm 1 are in order:

Remark 1 (Target Detection). *Equation (21) presents a threshold test requiring the search over a three dimensional grids composed of $|\Omega|$ slices of the $N \times M$ Doppler-delay grid. In order to keep the complexity low, we consider the Doppler-delay grid Γ defined in Section II-A and a coarse Ω .³ Even if this assumption is rather restrictive, it provides a computationally feasible and fast coarse estimation (step 1 of Algorithm 1), to be used as a baseline for the successive super-resolution ML-based parameter estimation (step 2 of Algorithm 1).*

³For instance, with an angular sector covering of 60 degrees divided in 4 equally spaced parts, the set of angles results to be (suppressing the center of the beam to be at 0 degree) $\Omega = \{[-30, -15], [-15, 0], [0, 15], [15, 30]\}$.

Algorithm 1: Joint Detection and Radar Parameters Estimation

Result: Target detection and radar parameter estimation.

Initialization: Set $\mathbf{y}' = \mathbf{y}$; Detected targets $N_{\text{dt}} = 0$;

Repeat

1) Detection / (AOA, Doppler, Delay) Coarse Estimation: Given \mathbf{y}' , search a possible set of targets

$$\mathcal{P} = \left\{ \max_{(\tau, \nu)} S_p(\tau, \nu, \phi) > T_r \right\}, \quad (21)$$

$$\text{s.t. } \left\{ \forall (\tau, \nu, \phi) \in \Gamma \times \Omega \right\},$$

where T_r is the detection threshold, to be properly optimized, Γ is the Doppler-delay grid described in II-A and Ω is defined as a discretized set of angles. The p -th target is associated to a coarse estimation $(\hat{\phi}_p, \hat{\tau}_p, \hat{\nu}_p)$, such that $S_p(\hat{\phi}_p, \hat{\tau}_p, \hat{\nu}_p)$ is above the threshold and is a local maximum;

2) Super-Resolution Parameter Estimation:

2.1) Fine AOA:

$$\hat{\phi}_p = \arg \max_{\phi} S_p(\hat{\tau}_p, \hat{\nu}_p, \phi), \quad p = 1, \dots, |\mathcal{P}|. \quad (22)$$

2.2) Fine Doppler-delay Estimation:

Initialization: Iteration $i = 0$, initialize $\hat{h}'_p[0] = 0$.

For Iteration $i = 1, 2, \dots$ **do**

• **Delay and Doppler update:** Find the estimates $\hat{\tau}_p[i], \hat{\nu}_p[i]$ by solving the two-dimensional maximization

$$(\hat{\tau}_p[i], \hat{\nu}_p[i]) = \arg \max_{(\tau, \nu)} \left\{ S_p - I_p \right\}, \quad (23)$$

with S_p and I_p computed for $(\hat{h}'_p[i], \tau, \nu, \hat{\phi}_p[i])$;

• **Complex channel coefficients update:** Solve the linear system (17) using channel matrices \mathbf{G}_p with parameters $(\hat{h}'_p[i], \hat{\tau}_p[i], \hat{\nu}_p[i], \hat{\phi}_p)$, and let the solution be denoted by $\hat{h}'_p[i]$;

End

3) Re-Fine AOA: Compute (22) using the refined estimation $(\hat{\tau}_p, \hat{\nu}_p)$ obtained in (23);

4) SIC: Compute

$$\mathbf{y}' = \mathbf{y} - \sum_{p=0}^{|\mathcal{P}|} \left[\hat{h}'_p \mathbf{G}_p(\hat{\tau}_p, \hat{\nu}_p, \hat{\phi}_p) \right] \mathbf{x}, \quad (24)$$

increase targets counter $N_{\text{dt}} = N_{\text{dt}} + |\mathcal{P}|$;

Until Stopping Criterion;

Remark 2 (Fine AoA Estimation). *Since S_p is a convex function in ϕ for a fixed pair (τ_p, ν_p) , the result of (22) can be exactly computed using common convex solvers. Therefore, the angle can be estimated with super-resolution far beyond the discrete grid Ω .*

Remark 3. *The magnitude of S_p strictly depends on the target range (and pathloss). Thus, in order to keep a fixed threshold T_r for all iterations, the argument $\max_{(\tau, \nu)} S_p(\tau, \nu, \phi)$ has to be normalized at each iteration, for instance, w.r.t. its mean computed over all possible angles.*

TABLE I: System parameters

$N = 6$	$M = 512$
$f_c = 24.25$ [GHz]	$B = 150$ [MHz]
$v_{\text{res}} \simeq 440$ [km/h]	$r_{\text{res}} \simeq 1$ [m]
$v_{\text{max}} = N \cdot v_{\text{res}}$	$r_{\text{max}} = M \cdot r_{\text{res}}$
$P_{\text{avg}} = 40$ [mW]	$\sigma_{\text{rcs}} = 1$ [m ²]
Noise Figure = 3 [dB]	Noise PSD = $2 \cdot 10^{-21}$ [W/Hz]
$N_a = 16, 32, 64, 128$	$N_{\text{rf}} = 8$

B. Reduced-Complexity Parameter Estimation

In the target tracking phase, the matrix \mathbf{G}_p in (13) shall be updated dynamically as the BF matrix \mathbf{F} of dimension $N_a \times N_{\text{rf}}$ and the channel matrix $\mathbf{\Psi}^p$ of $NM \times NM$ change in time. The following solution can be adopted in order to reduce the computational complexity related to the dynamically changing matrices. Namely, we compute \mathbf{G}_p for target p by selecting only the column of \mathbf{F} corresponding to this target already detected in Step 1 of Algorithm 1. Assuming that targets are located with different ranges from the radar, this low-complexity method does not affect the parameter estimation performance. If there are a few targets located with a similar range from the radar, they can be grouped together within the same narrow beam.

C. Cramér-Rao Lower Bound (CRLB)

We consider the CRLB as a theoretical benchmark. In order to estimate a complex channel coefficient, we let $A_p = |h'_p|$ and $\psi_p = \angle(h'_p)$ denote the amplitude and the phase of h'_p , respectively. Thus, $5P$ real variables have to be estimated, i.e., $\boldsymbol{\theta} = \{A_p, \psi_p, \tau_p, \nu_p, \phi_p\}$. We form the $5P \times 5P$ Fisher information matrix whose (i, j) element is

$$[\mathbf{I}(\boldsymbol{\theta})]_{i,j} = \frac{2}{N_0} \text{Re} \left\{ \sum_{n,m,t} \left[\frac{\partial s_p^{[n,m,t]}}{\partial \theta_i} \right]^* \left[\frac{\partial s_q^{[n,m,t]}}{\partial \theta_j} \right] \right\}, \quad (25)$$

where $p = [i]_P$, $q = [j]_P$, and

$$s_p^{[n,m,t]} = A_p e^{j\psi_p} b_t(\phi_p) a_t^*(\phi_p) f_t \sum_{k,l} \Psi_{n,k}^p[m, l] x_{k,l}, \quad (26)$$

where (n, m, t) denote time, subcarrier, and antenna, respectively, while f_t is the t -th entry of the BF vector of any RF chain.⁴ Note that, even if not explicitly indicated for the sake of simplicity, the summations w.r.t. k and l extend from 0 to $N - 1$ and $M - 1$, respectively, as in all previous analysis. The desired CRLB is obtained taking the diagonal elements of the inverse Fisher information matrix, filled with the corresponding derivatives.

IV. NUMERICAL RESULTS

We set the number of RF chains to $N_{\text{rf}} = 8$, such that a single equipment is able to jointly track and communicate to N_{rf} separately targets (or groups of targets), while $N_{\text{rf}} \ll N_a$. Table I provides all the system parameters.

⁴Here we assume that, given a proper BF design, the beam patterns directed to different targets do not interfere. Hence, we completely neglect beam interference, and only a BF vector entry f_t appears at a time.

In our simulations, we rely on the following assumptions:

- Given the choice of a mmWave communication, we assume a single LoS path between the Tx and the radar target [25], [26], [9]. This is motivated by the fact that any possible scattering component different from the LoS generally brings much lower power, given by additional reflections of the echo signal.
- Any backscattered power to the radar Rx is considered as a possible target. The objective is to sense the surrounding environment, and the differentiation between active targets and obstacles is a post-processing decision. Clearly, in a second phase, communication is established only towards active targets.
- We consider the complete blockage of the signal propagation to the first object hit. This assumption is completely fulfilled in mmWave communication scenarios.⁵

Note that the aforementioned assumption are shared by many works in literature (see, e.g., [9] and references therein).

The radar two-way pathloss is defined as [6, Chapter 2]

$$PL = \frac{(4\pi)^3 r^4}{\lambda^2}, \quad (27)$$

and the definition of the radar SNR becomes

$$SNR = \frac{\lambda^2 \sigma_{\text{rcs}} G_{\text{Tx}} G_{\text{Rx}} P_{\text{avg}}}{(4\pi)^3 r^4 \sigma_w^2}, \quad (28)$$

where $\lambda = c/f_c$ is the wavelength, c is the speed of light, σ_{rcs} is the radar cross-section of the target in m^2 , G_{Tx} and G_{Rx} are the antenna gains at the Tx and Rx respectively, r is the distance between Tx and Rx, and σ_w^2 is the variance of the AWGN noise with noise power spectral density (PSD) of $2 \cdot 10^{-21}$ [W/Hz]. We choose $\sigma_{\text{rcs}} = 1$ [m^2], while different choices can be found in literature [31], [32]. Note that, while G_{Tx} can change with the operational mode, G_{Rx} is kept constant (within the angular sector of interest) in order to allow isotropic reception, as already explained. Information about antenna gains, beam patterns, two-way (Tx and Rx) beamwidth, and more antenna basics (also for mono-static radars) can be found, for instance, in [33], [4]. The detection threshold T_r in Algorithm 1 has been numerically evaluated in order to have a false alarm probability of 10^{-4} (as done, e.g., in [9]).

While two distinct targets in the angle domain can be identified if the angular resolution meets some conditions (depending on the number of antennas, the angular distance between the two targets, and the antenna array properties) [6]. The velocity and the range resolution is determined by the system parameters in Table I and given by

$$v_{\text{res}} = \frac{Bc}{2NMf_c} [\text{m/s}], \quad r_{\text{res}} = \frac{c}{2B} [\text{m}]. \quad (29)$$

In order to get a reasonable range resolution, e.g., < 1 [m], a large bandwidth has to be considered.⁶ Since the velocity

⁵Note that the proposed algorithm could be able to correctly distinguish more targets sharing the same angular direction, if separated in at least one other domain (Doppler or delay) [12].

⁶Note that a tradeoff appears. Larger bandwidths mean more precise resolution, but lower theoretical maximum range (with the same $N \times M$ grid). We remark that our algorithm is completely independent of these choices.

resolution is directly proportional to B , for a fixed f_c , the only way to obtain lower values is to increase the block size NM , leading to a remarkable increase in computational complexity, which could be not affordable. For this reason, we set the system parameters by focusing on a reasonable range resolution (and theoretical maximum range) under a feasible computational complexity. Note that the maximum range could not be achieved if the backscattered power is below the noise floor. However, the chosen system setup leads to an unavoidable very large velocity resolution. Under the aforementioned assumptions, taken at the beginning of Section IV, the problem of targets identifiability appears only in the angular domain. However, this only happens at mmWave, thus, range and velocity resolutions are reported here for completeness, since the proposed scheme could target lower frequencies, where the aforementioned assumption might not be satisfied.

Remark 4. *The parameter estimation performance of the proposed ML-based algorithm, in particular range and velocity estimation, strictly depends on the dimension of the block of data sent, i.e., the product $N \cdot M$. Thus, the system parameters of Tab. I can be easily tuned to achieve the desired levels of radar resolutions (modifying the bandwidth), acquisition time (based on the length of the OTFS frame in time), maximum range, etc. Clearly, the CRLB changes accordingly. Moreover, note that this is also possible thanks to OTFS modulation, which is not sensitive to Doppler and delay effects.*

Remark 5. *The (radar) range and velocity resolution in (29) indicates the minimum necessary targets spacing, in one of the two domain, such that both of them are distinguishable at the radar Rx. This is not linked to the performance of our ML-based detector, which is able to estimate the parameters accurately far beyond the resolution in (29). Thus, there is a huge difference between targets identifiability and estimation performance.*

A. Simulation Results

Fig. 3 shows the radar performance in terms of probability of detection (PD), range/velocity/AoA estimation during the detection phase (Fig.1a). When more than one target is considered within the simulation scenario, the PD P_d is averaged w.r.t. all P targets, i.e.,

$$P_d = \frac{\sum_{p=0}^{P-1} P_d(p)}{P}, \quad (30)$$

where $P_d(p)$ denoted the PD of the p -th target.

First, note that, by considering an angular coverage of 10° degrees (blue line), the maximum range to correctly identify a target, limited by the pathloss and thus different from the theoretical limit indicated in Table I, is about 110 m. For any distance between Tx and target, the estimation performance of radar parameters of interest (range, velocity, and AoA) follows the corresponding CRLB. More in details, note that at the limit range of 110 m, the root MSE (RMSE) for range, velocity, and angle are respectively, $\simeq 4 \cdot 10^{-2}$ [m], $\simeq 1.6 \cdot 10^1$ [m/s], $\simeq 4 \cdot 10^{-2}$ [degree $^\circ$]. As expected, given the system

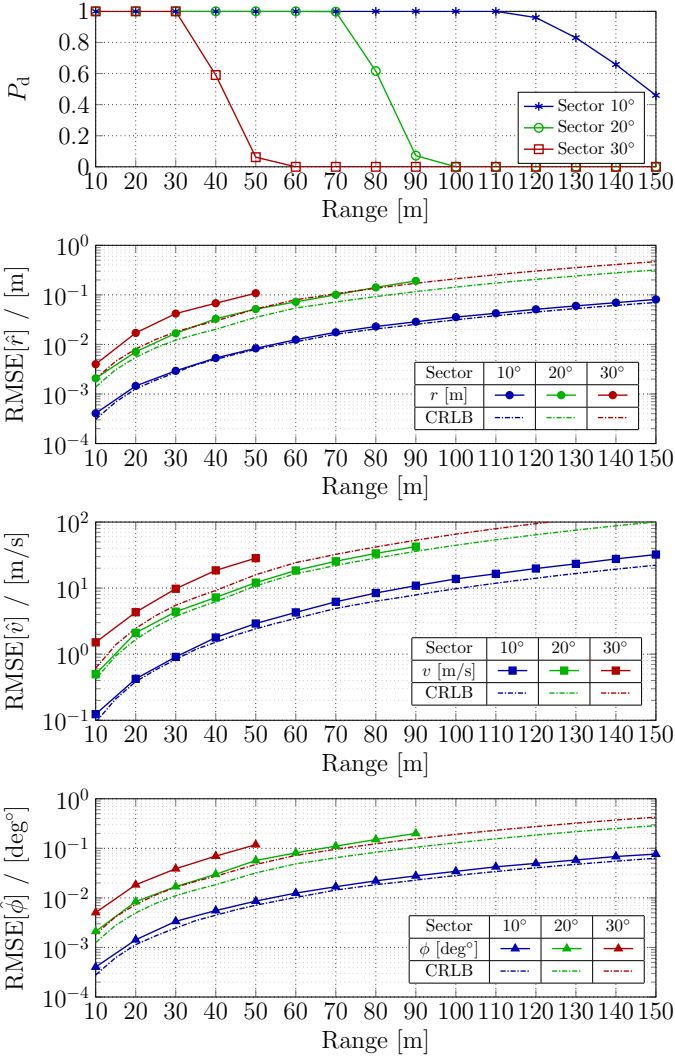


Fig. 3: Detection phase. Single target at a different distance within the illuminated angular sector of specified coverage. RMSE performance with associated CRLB and detection performance. $N_a = 128$.

parameters, the velocity RMSE is quite poor, while the others estimation performance are satisfactory. However, a proper BF design towards targets, in a subsequent tracking phase, could improve the estimation performance maximizing the received SNR, as showed in next results. As seen from Fig. 3, by increasing the angle sector from 10° to 30° degrees, the backscattered power gets smaller (less BF gain), hence the maximum range significantly decreases. There exists a non-trivial tradeoff between the width of beams and radar performance. Wider angular sectors allow to explore the environment in less time, but with limited maximum range, while narrower sectors maximize the received power and the maximum target range, at the cost of a time consuming beam sweeping search. Clearly, RMSE performance can not be computed if the PD is equal to 0, i.e., the target is not detected, thus RMSE curves may stop at certain ranges, as visible in Fig. 3.

Fig. 4 shows the performance of the SIC technique presented in Algorithm 1 during the detection phase in the

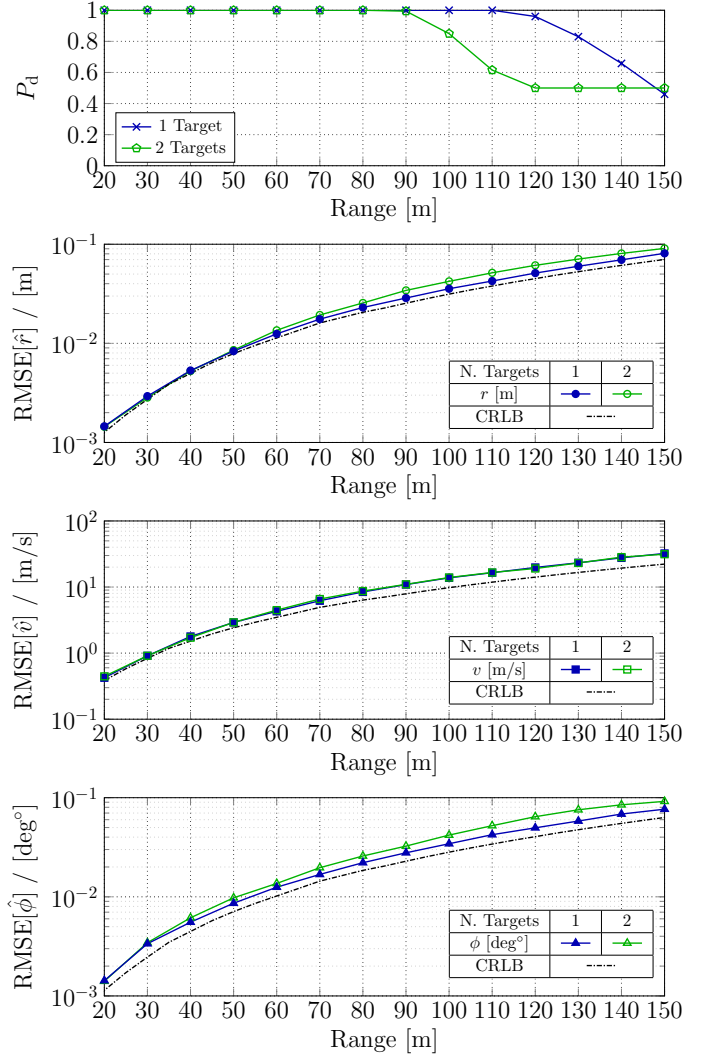


Fig. 4: Detection phase. Two target, one located at 10 [m] and the other moving at a different distance (x-axis) within the illuminated 10° angular sector as shown in Fig. 5. RMSE performance with associated CRLB. Detection performance. $N_a = 128$.

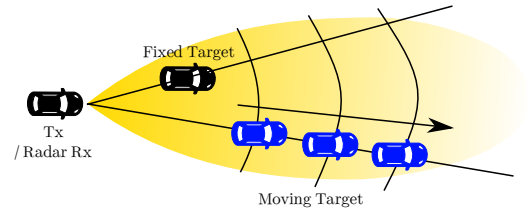


Fig. 5: Example of scenario depicted in Fig. 4. The fixed target (in black) masks the moving target, in blue, which changes its location within the illuminated angular sector.

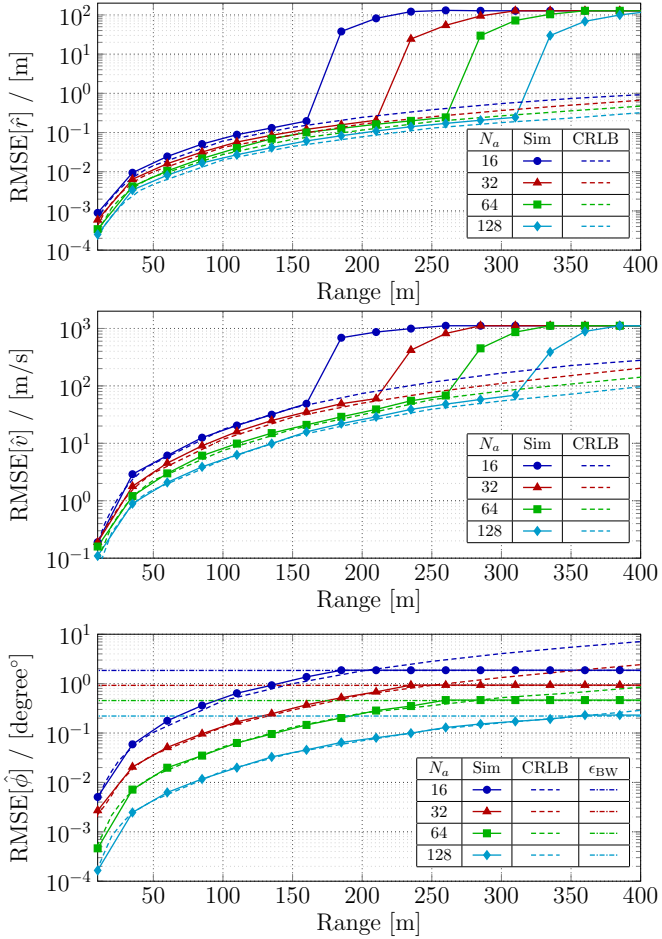


Fig. 6: Tracking scenario. Tx BF distinct beams towards three different targets.

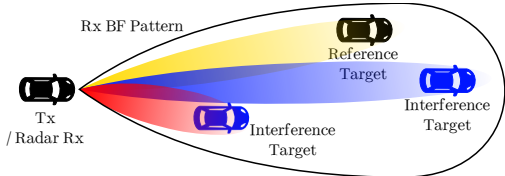


Fig. 7: Example of scenario depicted in Fig. 6. The goal is to correctly estimate the parameters of the reference target (in black), while interference targets (in blue) lay within the same Rx BF pattern (depicted in Fig. 2 and with the black shape in this figure).

scenario depicted in Fig. 5. Namely, the transmitter wishes to detect two targets, one at fixed distance of 10 [m], the other with moving w.r.t. the x-axis, i.e., from 20 to 150 [m] (see Fig. 5). SIC is necessary because the closer target (black car) will mask the further target (blue car) so that the latter cannot be detected. First, the first plot of Fig. 4, referred to the PD, shows that, when the moving target is located at ranges greater than 90 [m], corresponding to the relative range beyond 80 [m], the masking effect is not removed efficiently by the SIC technique (the residual interference is remarkable), and the target at longer distance is not detected correctly. In fact,

at the extreme point, the curve flats to $P_d = 0.5$, because only one target out of two (clearly, the closet to the radar Rx, i.e., the one fixed at 10 [m]) is correctly detected. As clearly visible, the performance in terms of RMSE, which considers in this case the estimation performance averaged w.r.t. the detected targets (note that the target located at 10 [m] is always detected correctly), slightly changes while considering one or two targets, as a confirmation of the effectiveness of the proposed algorithm. Note that the blue curves of Fig. 4 correspond to the blue ones of Fig. 3.

Now we consider the tracking phase corresponding to Fig. 1b. The scenario takes into account one Tx and three targets within an angular sector of 10° degrees, as shown in Fig. 7. Fig. 6 shows the RMSE performance of the reference target (black car) in the presence of other two targets (blue cars). Note that distance, velocity, and angular position of all three targets are randomly chosen at every Monte Carlo iteration, in such a way the complete masking effect presented in Fig. 4 does not occur, and an average of RMSE results is finally computed. From Fig. 6, we observe that the RMSE critically depends on the number of antennas. This is because the BF gain grows proportionally with the number of antennas and increases the backscattered signal power. Moreover, note that a (reversed) “waterfall” behavior is shown for range and velocity estimation. This is because, even if the presence of the target is given for granted, low SNR values might still lead to a large error during the Doppler-delay ML maximization (see Algorithm 1). The waterfall behavior is typical of ML estimators and has been extensively analyzed in [11]. Also note that the AoA RMSE performance is upper limited by the 3-dB beamwidth of the beam pattern (see, e.g., [4], [33]). In fact, supposing that the target position lies within the 3-dB beamwidth, also the initial AoA estimation (the upper and lower limit of matrix Ω in (21)) is limited to that width. As a consequence, the RMSE does not exceed a systematic error, indicated as ϵ_{BW} , calculated by averaging over random AoA estimation realizations within the range of possibilities, i.e., between the upper and lower limit set by the 3-dB beamwidth of the beam pattern.

V. CONCLUSIONS

In this paper, we proposed an efficient ML-based algorithm able to jointly perform target detection and radar parameters estimation, i.e., range, velocity, and AoA, by using a MIMO mono-static radar adopting OTFS modulation and operating in different modes. Simulation results demonstrate the robustness of the algorithm in term of both target identifiability and estimation by exploiting a SIC mechanism. Interestingly, our proposed scheme is able to simultaneously send data streams between one to the number of RF chains, depending on different operational phases. There are a couple of interesting directions which are left as future works. These include the further optimization of the hybrid beamforming matrices, the comparison with other radar or/and communication waveforms, efficient target tracking method following some mobility models.

VI. ACKNOWLEDGMENT

The work of Lorenzo Gaudio, Giuseppe Caire, and Giulio Colavolpe is supported by Fondazione Cariparma, under the TeachInParma Project. This research benefits from the HPC (High Performance Computing) facility of the University of Parma, Italy.

REFERENCES

- [1] J. Li and P. Stoica, *MIMO radar signal processing*. John Wiley & Sons, 2008.
- [2] S. M. Patole, M. Torlak, D. Wang, and M. Ali, "Automotive radars: A review of signal processing techniques," *IEEE Signal Process. Mag.*, vol. 34, no. 2, pp. 22–35, March 2017.
- [3] X. Song, S. Haghighatshoar, and G. Caire, "A scalable and statistically robust beam alignment technique for millimeter-wave systems," *IEEE Trans. Wireless Commun.*, vol. 17, no. 7, pp. 4792–4805, 2018.
- [4] B. Friedlander, "On transmit beamforming for MIMO radar," *IEEE Trans. Aerosp. Electron. Syst.*, vol. 48, no. 4, pp. 3376–3388, 2012.
- [5] U. Niesen and J. Unnikrishnan, "Joint beamforming and association design for MIMO radar," *IEEE Trans. Signal Process.*, vol. 67, no. 14, pp. 3663–3675, 2019.
- [6] M. A. Richards, *Fundamentals of radar signal processing, Second edition*. McGraw-Hill Education, 2014.
- [7] Y. Bar-Shalom and X.-R. Li, *Multitarget-multisensor tracking: principles and techniques*. YBs Storrs, CT, 1995, vol. 19.
- [8] S. Buzzi, C. D'Andrea, and M. Lops, "Using massive MIMO arrays for joint communication and sensing," in *2019 53rd Asilomar Conference on Signals, Systems, and Computers*, 2019, pp. 5–9.
- [9] E. Grossi, M. Lops, L. Venturino, and A. Zappone, "Opportunistic radar in IEEE 802.11ad networks," *IEEE Trans. Signal Process.*, vol. 66, no. 9, pp. 2441–2454, May 2018.
- [10] S. Fortunati, L. Sanguineti, F. Gini, M. S. Greco, and B. Himed, "Massive MIMO radar for target detection," *IEEE Trans. Signal Process.*, vol. 68, pp. 859–871, 2020.
- [11] L. Gaudio, M. Kobayashi, G. Caire, and G. Colavolpe, "On the effectiveness of OTFS for joint radar parameter estimation and communication," *IEEE Transactions on Wireless Communications*, pp. 1–1, 2020.
- [12] L. Gaudio, M. Kobayashi, G. Caire, and G. Colavolpe, "Joint radar target detection and parameter estimation with MIMO OTFS," *arXiv preprint arXiv:2004.11035*, 2020.
- [13] R. Hadani, S. Rakib, M. Tsatsanis, A. Monk, A. J. Goldsmith, A. F. Molisch, and R. Calderbank, "Orthogonal time frequency space modulation," in *2017 IEEE Wireless Commun. and Network. Conf. (WCNC)*. IEEE, 2017, pp. 1–6.
- [14] W. Shen, L. Dai, J. An, P. Fan, and R. W. Heath, "Channel estimation for orthogonal time frequency space (OTFS) massive MIMO," *IEEE Transactions on Signal Processing*, vol. 67, no. 16, pp. 4204–4217, 2019.
- [15] M. Kollengode Ramachandran and A. Chockalingam, "MIMO-OTFS in high-doppler fading channels: Signal detection and channel estimation," in *2018 IEEE Global Communications Conference (GLOBECOM)*, 2018, pp. 206–212.
- [16] S. H. Dokhanchi, B. S. Mysore, K. V. Mishra, and B. Ottersten, "A mmWave automotive joint radar-communications system," *IEEE Trans. Aerosp. Electron. Syst.*, vol. 55, no. 3, pp. 1241–1260, June 2019.
- [17] L. Zheng, M. Lops, Y. C. Eldar, and X. Wang, "Radar and communication coexistence: An overview: A review of recent methods," *IEEE Signal Processing Magazine*, vol. 36, no. 5, pp. 85–99, 2019.
- [18] A. Hassanien, M. G. Amin, E. Aboutanios, and B. Himed, "Dual-function radar communication systems: A solution to the spectrum congestion problem," *IEEE Signal Process. Mag.*, vol. 36, no. 5, pp. 115–126, Sep. 2019.
- [19] P. Raviteja, K. T. Phan, Y. Hong, and E. Viterbo, "Orthogonal time frequency space (OTFS) modulation based radar system," in *2019 IEEE Radar Conf. (RadarConf)*. IEEE, 2019, pp. 1–6.
- [20] X. Song, T. Kühne, and G. Caire, "Fully-/partially-connected hybrid beamforming architectures for mmWave MU-MIMO," *IEEE Trans. Wireless Commun.*, vol. 19, no. 3, pp. 1754–1769, 2020.
- [21] Z. Chen, Z. Cao, X. He, Y. Jin, J. Li, and P. Chen, "DoA and DoD estimation and hybrid beamforming for radar-aided mmWave MIMO vehicular communication systems," *Electronics*, vol. 7, no. 3, p. 40, 2018.
- [22] A. Sabharwal, P. Schniter, D. Guo, D. W. Bliss, S. Rangarajan, and R. Wichman, "In-band full-duplex wireless: Challenges and opportunities," *IEEE J. Sel. Areas Commun.*, vol. 32, no. 9, pp. 1637–1652, Sep. 2014.
- [23] S. M. Wentworth, *Applied electromagnetics: early transmission lines approach*. John Wiley & Sons, 2007.
- [24] M. Duarte and A. Sabharwal, "Full-duplex wireless communications using off-the-shelf radios: Feasibility and first results," in *2010 Conference Record of the Forty Fourth Asilomar Conference on Signals, Systems and Computers*, 2010, pp. 1558–1562.
- [25] P. Kumari, J. Choi, N. Gonzalez-Prelcic, and R. W. Heath, "IEEE 802.11ad-based radar: An approach to joint vehicular communication-radar system," *IEEE Trans. Veh. Technol.*, vol. 67, no. 4, pp. 3012–3027, April 2018.
- [26] D. H. N. Nguyen and R. W. Heath, "Delay and Doppler processing for multi-target detection with IEEE 802.11 OFDM signaling," in *Proc. IEEE Int. Conf. Acoustics, Speech, and Signal Processing (ICASSP)*, March 2017, pp. 3414–3418.
- [27] G. A. Vitetta, D. P. Taylor, G. Colavolpe, F. Pancaldi, and P. A. Martin, *Wireless communications: algorithmic techniques*. John Wiley & Sons, 2013.
- [28] P. Raviteja, K. T. Phan, Y. Hong, and E. Viterbo, "Interference cancellation and iterative detection for orthogonal time frequency space modulation," *IEEE Trans. Wireless Commun.*, vol. 17, no. 10, pp. 6501–6515, Oct 2018.
- [29] F. Gini, A. De Maio, and L. Patton, *Waveform design and diversity for advanced radar systems*. Institution of engineering and technology London, UK, 2012.
- [30] G. Matz, H. Bolcskei, and F. Hlawatsch, "Time-frequency foundations of communications: Concepts and tools," *IEEE Signal Process. Mag.*, vol. 30, no. 6, pp. 87–96, Nov 2013.
- [31] H. Suzuki, "Measurement results of radar cross section of automobiles for millimeter wave band," in *Proceedings of the 7th World Congress on Intelligent Systems*, 2000.
- [32] E. Bel Kamel, A. Peden, and P. Pajusco, "RCS modeling and measurements for automotive radar applications in the W band," in *2017 11th European Conference on Antennas and Propagation (EUCAP)*, 2017, pp. 2445–2449.
- [33] H. J. Visser, *Array and phased array antenna basics*. John Wiley & Sons, 2006.